Equilibrium thermal vibrations of carbon nanotubes

Edward H. Feng* and Reese E. Jones
Sandia National Laboratories, Livermore, California 94551-0969, USA
(Received 4 February 2010; published 26 March 2010)

An understanding of thermal vibrations of carbon nanotubes is key to their application as high-frequency mechanical resonators. To this end, we calculate the free thermal vibrations of cantilevered carbon nanotubes using molecular dynamics and explain the resulting power spectral density of the tip displacement with equilibrium statistical mechanics and continuum beam theory.

DOI: 10.1103/PhysRevB.81.125436 PACS number(s): 63.22.−m, 61.48.De, 62.25.Jk

I. INTRODUCTION

Unlike the silicon cantilever in an atomic force microscope (AFM), the thermal vibrations of an anchored carbon nanotube (CNT) can be significant compared to its radius.[1] Experimental measurements of these intrinsic vibrations along with continuum beam theory allow one to estimate the CNT's stiffness.[1,2] Moreover, the thermal vibrations are closely linked to the resonance properties of the CNT (Refs. 3–6) as they serve as a source of self-excitation and noise in determining natural frequencies. These resonance properties play a crucial role in using a CNT cantilever as a nanomechanical sensor and have recently enabled the mass measurement of a single gold atom.[7] Cantilever structures are also a key component in the AFM, which can manipulate a single molecule. Efforts to obtain a more sensitive AFM through smaller cantilevers[8,9] suggests that a single CNT may replace the usual silicon-based AFM cantilever. A fundamental step toward this next generation sensor is characterizing the noise that arises from the thermal vibrations with the intent to ultimately mitigate its effects.

To this end, we calculate the free thermal vibrations of a CNT cantilever with molecular-dynamics (MD) simulations. Much like early experimental work on AFM cantilevers,[8,9] we track the CNT's tip as a function of time and calculate the Fourier spectrum of its displacement. While previous work has used MD to investigate other properties of a suspended CNT,[10–13] this is the first calculation of this thermal vibrational spectrum. Our MD results show a rich diversity of features not apparent from current experiments, which include a discrete set of higher-order peaks in addition to a peak that corresponds to the fundamental mode of vibration. Inspired by the pioneering work of Treacy *et al.*,[1,2] we analyze the spectrum with equilibrium statistical mechanics and continuum beam theory which provides a coarse-grained model for the long-wavelength transverse phonons. The Timoshenko beam theory, a generalization of the commonly used Euler-Bernoulli (EB) theory, provides an excellent quantitative description of the frequency and intensity of the discrete peaks of the vibrational spectrum. Moreover, the MD results also shows finite-temperature features not captured by continuum beam theory such as the spreading of the peaks and a scaling at high frequency that indicates diffusive motion of the tip.

II. BEAM THEORY

Since understanding the free vibration of a CNT cantilever is essentially a study of its dynamics, we assume that it behaves like a continuum tube governed by Timoshenko beam theory.[14] For a beam with its primary axis along the x direction, its kinematics are described by its transverse displacement $y(x,t)$ and its angular rotation $\phi(x,t)$ in the (x,y) plane for all times t. This description applies to both dimensions, y and z, transverse to the beam. These fields must satisfy Euler's balances for linear and angular momentum

$$\rho A\frac{\partial^2 y}{\partial t^2} = -\frac{\partial}{\partial x}\left[kAG\left(\phi - \frac{\partial y}{\partial x}\right)\right], \tag{1}$$

$$\rho I\frac{\partial^2 \phi}{\partial t^2} = EI\frac{\partial^2 \phi}{\partial x^2} - kAG\left(\phi - \frac{\partial y}{\partial x}\right), \tag{2}$$

where ρ is the density in mass per unit volume, A is the cross-sectional area, I is the area moment of inertia of the cross section, and G and E are the shear and Young's moduli, respectively. In addition, k is a geometric factor called the Timoshenko shear coefficient that depends on the shape of the cross section.[14,15] In the Timoshenko theory, the shear force $Q=-kAG(\phi-\frac{\partial y}{\partial x})$ results from the difference in the angular rotation and the slope of the displacement. For a cantilever of length L, the boundary conditions at the fixed end correspond to a fixed displacement $y(0,t)=0$ and rotation $\phi(0,t)=0$, while at the free end we assume no moment $M(L,t)=-EI\frac{\partial\phi(L,t)}{\partial x}=0$ and a shear force $Q(L,t)=f$.

We first consider the static deflection of the cantilever due to a tip force f by setting the time derivatives to zero in Eqs. (1) and (2). For the tip displacement $u\equiv y(L)$, the solution $u=\frac{1}{K}f$ is linear in the force with spring constant

$$K = \frac{EI}{L^3}\frac{3}{1+3\kappa/\epsilon^2}$$

in which $\kappa\equiv E/(kG)$ is a measure of the normal stiffness relative to the shear stiffness and $\epsilon\equiv L/\sqrt{I/A}$ is an aspect ratio for the beam. With the applied force f, the tip can only be at mechanical equilibrium at u if the rest of the beam exerts a restoring force $-Ku$ on it. We can assume this force results from a harmonic potential $U=\frac{1}{2}Ku^2$ on the tip. In thermal equilibrium at a temperature T, the Boltzmann-Gibbs distribution states that the probability of a displacement u is

$Z^{-1}e^{-Ku^2/(2k_BT)}$ in which $Z=\int_{-\infty}^{\infty}e^{-Ku^2/(2k_BT)}du$ and k_B is Boltzmann's constant.[16] This implies the ensemble average of the square of the tip displacement is

$$\langle u^2\rangle = \frac{k_BT}{K} = \frac{L^3}{3EI}\left(1+\frac{3\kappa}{\epsilon^2}\right)k_BT. \tag{3}$$

As $\epsilon\to\infty$, we recover the result for $\langle u^2\rangle$ derived from EB theory and used to analyze experiments on the thermal vibration of a CNT cantilever.[1,2]

To understand the free thermal vibration of the CNT, we return to the time-dependent motion of the cantilever in Eqs. (1) and (2) with no force on the free end. Taking the partial derivative of Eq. (2) with respect to x and using Eq. (1) to evaluate the partial derivatives of ϕ in the result, we obtain

$$\frac{\partial^2\bar{y}}{\partial\tau^2}+\frac{\partial^4\bar{y}}{\partial\xi^4}-\epsilon^{-2}(1+\kappa)\frac{\partial^4\bar{y}}{\partial\xi^2\,\partial\,\tau^2}+\kappa\epsilon^{-4}\frac{\partial^4\bar{y}}{\partial\tau^4}=0. \tag{4}$$

Here, we use dimensionless length $\xi=x/L$, displacement $\bar{y}=y/L$, and time $\tau=t\varpi$ in which L is the length of the beam and $\varpi=\sqrt{EI/(\rho A)}L^{-2}$ is a characteristic frequency. As the aspect ratio $\epsilon\to\infty$ diverges in Eq. (4), we recover the dynamical equation for an EB beam. A similar analysis gives

$$\frac{\partial^2\phi}{\partial\tau^2}+\frac{\partial^4\phi}{\partial\xi^4}-\epsilon^{-2}(1+\kappa)\frac{\partial^4\phi}{\partial\xi^2\,\partial\,\tau^2}+\kappa\epsilon^{-4}\frac{\partial^4\phi}{\partial\tau^4}=0 \tag{5}$$

for the angular rotation.

Huang[17] derived the separable solutions $\bar{y}(\xi,\tau)=e^{i\Omega\tau}Y(\xi)$ and $\phi(\xi,\tau)=e^{i\Omega\tau}\Phi(\xi)$ to Eqs. (4) and (5), respectively, for dimensionless frequency Ω. For low frequencies $\Omega<\epsilon^2\kappa^{-1/2}$, $Y(\xi)$ and $\Phi(\xi)$ are linear combinations of $\cosh(\alpha\xi)$, $\sinh(\alpha\xi)$, $\cos(\beta\xi)$, and $\sin(\beta\xi)$ with dimensionless wave vectors

$$\begin{matrix}\alpha^2\\ \beta^2\end{matrix} = \frac{\Omega}{2}\left(\frac{\Omega}{\epsilon^2}\right)\left[\sqrt{(1-\kappa)^2+4\left(\frac{\Omega}{\epsilon^2}\right)^{-2}}\mp(1+\kappa)\right].$$

Applying the boundary conditions for a cantilever leads to the characteristic equation

$$2+\left[\left(\frac{\Omega}{\epsilon^2}\right)^2(1-\kappa)^2+2\right]\cosh\alpha\cos\beta - \frac{(1+\kappa)}{\sqrt{\left(\frac{\Omega}{\epsilon^2}\right)^{-2}-\kappa}}\sinh\alpha\sin\beta=0 \tag{6}$$

which reduces to the EB relation $1+\cosh\alpha\cos\alpha=0$ in the limit $\frac{\Omega}{\epsilon^2}\to 0$ of low frequencies and long aspect ratios. The discrete set of solutions $\Omega_0,\Omega_1,\ldots<\epsilon^2\kappa^{-1/2}$ to Eq. (6) give the characteristic frequencies of a Timoshenko beam. Then the general solutions for the displacement and rotation are

$$\bar{y}(\xi,\tau)=\sum_n a_n e^{i\Omega_n\tau}Y_n(\xi),$$

$$\phi(\xi,\tau)=\sum_n a_n e^{i\Omega_n\tau}\Phi_n(\xi)$$

in which a_n is the modal amplitude and

$$Y_n(\xi)=\gamma_n\theta_n(\cosh\alpha_n\xi-\lambda_n\zeta_n\delta_n\sinh\alpha_n\xi-\cos\beta_n\xi+\delta_n\sin\beta_n\xi),$$

$$\Phi_n(\xi)=\cosh\alpha_n\xi+\frac{\theta_n}{\lambda_n\zeta_n}\sinh\alpha_n\xi-\cos\beta_n\xi+\theta_n\sin\beta_n\xi$$

are the spatial eigenfunctions. Here, α_n,β_n are the wave vectors corresponding to the characteristic frequency Ω_n while the other constants

$$\lambda_n=\frac{\alpha_n}{\beta_n},$$

$$\zeta_n=\frac{1+\epsilon^2\alpha_n^2}{\kappa+\epsilon^2\alpha_n^2},$$

$$\delta_n=\frac{\lambda_n^{-1}\sinh\alpha_n-\sin\beta_n}{\zeta_n\cosh\alpha_n+\cos\beta_n},$$

$$\theta_n=-\frac{\lambda_n\sinh\alpha_n+\sin\beta_n}{\zeta_n^{-1}\cosh\alpha_n+\cos\beta_n},$$

also depend on the mode.

The elastic energy of the Timoshenko beam

$$U=\frac{1}{2}\frac{EI}{L}\int_0^1\left|\frac{\partial\phi}{\partial\xi}\right|^2d\xi+\frac{1}{2}kAGL\int_0^1\left|\phi-\frac{\partial\bar{y}}{\partial\xi}\right|^2d\xi$$

has two contributions from the normal and shear stress, respectively. Due to the orthogonality of the spatial eigenfunctions, one can show that $U=\frac{1}{2}\Sigma_nK_nu_n^2$ is the sum of harmonic potentials on the tip displacement of each mode $u_n=a_nLY_n(1)$. This sum over modes is a generic feature of linear systems.[18] Here, the spring constants are

$$K_n=mN_n\omega_n^2$$

in which $\omega_n=\Omega_n\varpi$ is the dimensional frequency and $m=\rho AL$ is the mass of the beam. The constant N_n,

$$N_n=\frac{1}{Y_n(1)^2\epsilon^2}\int_0^1(\Phi_n^2+\epsilon^2Y_n^2)d\xi \tag{7}$$

gives an effective mass N_nm for each mode. Using this energy in the Gibbs-Boltzmann distribution, the thermal amplitude for the n mode is

$$\langle u_n^2\rangle=\frac{k_BT}{K_n}=\frac{k_BT}{mN_n}\omega_n^{-2}. \tag{8}$$

This ensemble average is the Timoshenko beam theory prediction for the squared amplitude of the nth mode in the thermal vibrational spectrum. This reduces to the EB result[1,2] since $N_n\to\frac{1}{4}$ as $\epsilon\to\infty$. This amplitude is related to a spectral intensity,

$$I_u(\omega)=\sum_n\frac{k_BT}{mN_n}\omega^{-2}\delta(\omega-\omega_n) \tag{9}$$

by $\langle u_n^2\rangle\approx I_u(\omega_n)d\omega$. Here, $\delta(\omega)$ is the Dirac delta function.

III. COMPUTATIONAL METHODS

To simulate a nanotube with molecular dynamics, we construct a (10,10) CNT by first creating a graphene sheet with a carbon-carbon bond distance d and then rolling it into a tube with its axis along the x axis. For this CNT, there are layers of 20 atoms that all have the same x coordinate in the crystal structure. We construct a cantilever by fixing the positions of first four layers (80 carbon atoms) at one end of the tube while the remaining carbon atoms form an uncapped CNT of length L. The tip position u is the average position of the last layer of 20 atoms. Since the carbon atoms in our simulation interact through the Tersoff potential,[19,20] we use $d=0.14589$ nm because the more common $d=0.142$ nm does not correspond to the minimum energy configuration of this tube structure. This choice of d only affects the clamping of the tube. We performed MD simulations with $d=0.142$ nm for a CNT with $L=20$ nm and $T=300$ K and obtained the same results within error for all quantities presented in this work.

We use the stochastic Andersen thermostat[21] to generate states from the canonical ensemble at constant temperature. We also tried the deterministic Nose-Hoover algorithm to equilibrate the system but we encountered long relaxation times in the tip displacement due to the tendency for ballistic phonon transport in CNTs.[22] The Andersen thermostat, which changes the velocity of particles by choosing a new velocity from a Maxwell-Boltzmann distribution, promotes mixing of the phonon spectrum and a short relaxation time for the tip displacement. For CNTs of length 20 and 50 nm, the velocities of all carbon atoms change every 10 ps and 60 ps, respectively, which is approximately the period of the fundamental mode of vibration.

To calculate the thermal vibrational spectrum of a CNT, we use the states from the canonical ensemble as initial conditions for trajectories with constant energy dynamics.[23] This method of first sampling the ensemble and then performing a simulation according to the true Newtonian dynamics is standard in the study of liquids.[24] Trajectories for CNTs of length 20 and 50 nm lasted 1 ns and 2 ns, respectively. For each state j in the ensemble, the tip displacement $u_j(t_i)$ is sampled at 10 fs intervals during the constant energy dynamics. Since the tip displacement is the average over the positions of 20 carbon atoms, radially symmetric modes are filtered out. The thermal tip displacement spectrum is $\langle|u(\omega_k)|^2\rangle = N^{-1}\Sigma_{j=1}^{N}|u_j(\omega_k)|^2$ in which $u_j(\omega_k)$ is the normalized Fourier transform of $u_j(t_i)$. Here, $N=30$ is the number of initial states from the ensemble for both the 20 and 50 nm tubes. This ensemble average $\langle|u(\omega_k)|^2\rangle$ will be compared with the theoretical result in Eq. (8).

IV. RESULTS

The discrete points with error bars in Fig. 1 are MD results for the vibrational spectrum. Figures 1(a) and 1(b) correspond to a 50 nm CNT at $T=300$ K and a 20 nm CNT at $T=700$ K, respectively. Both spectra clearly have distinct peaks. The shorter CNT has a fundamental peak at a higher frequency; the shift in frequency is consistent with the characteristic frequency $\varpi=\sqrt{EI/(\rho A)}L^{-2}$. Both spectra also display a series of higher-order peaks with increasing frequency, a feature we will soon relate to the beam characteristics of the CNT. At frequencies larger than the fundamental peak but between neighboring peaks, the spectrum scales as ω^{-2}, a characteristic of Brownian motion. Hence, the ensemble averaged dynamics of the tip at $\omega \gg \omega_0$ is apparently diffusive with additional intensity due to the beam resonances of the CNT.

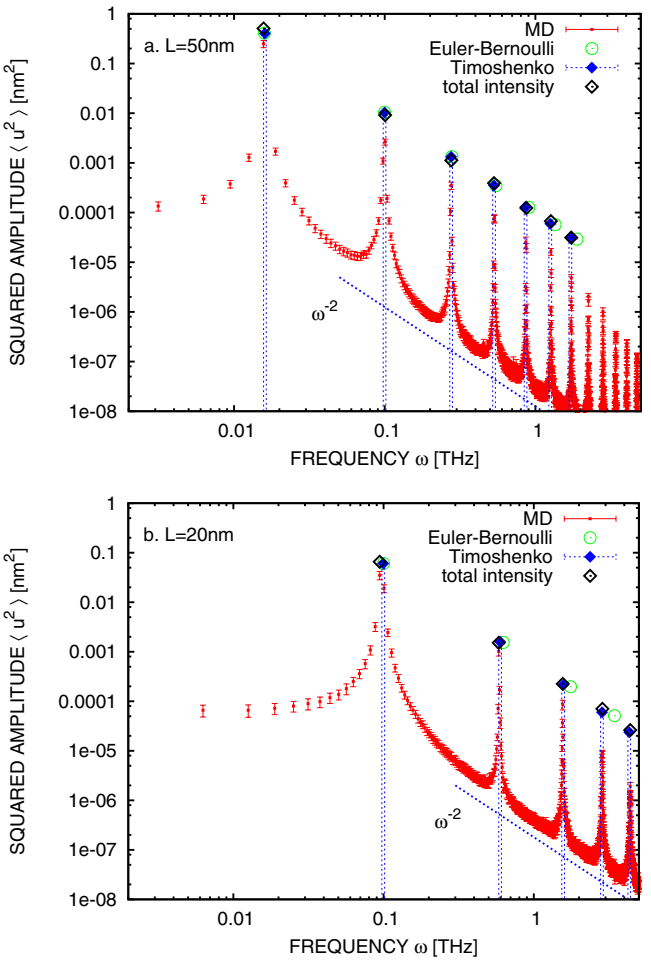

FIG. 1. (Color online) The thermal vibrational spectrum for (a) a 50 nm CNT at $T=300$ K and (b) a 20 nm CNT at $T=700$ K. The range of the axes in both plots is the same to facilitate comparison. In addition to the MD results, we display results from the Timoshenko and Euler Bernoulli beam theory. For the Timoshenko results, the width of the impulse is the error in the frequency prediction that results from uncertainty in estimating the flexural rigidity EI. The total intensity is the sum over the spectral intensity of the peak.

We would also like to make a quantitative comparison of the beam theory with the MD results. Since the predicted frequencies are proportional to the characteristic frequency $\varpi=\sqrt{EI/(\rho A)}L^{-2}$, we must first determine the flexural rigidity EI. Since Eq. (3) implies that EI is related to $\langle u^2\rangle$ as a function of T, we show this plot for a 20 nm CNT in Fig. 2. As dictated by the theory in Eq. (3), the best-fit line is constrained to pass through the origin. To obtain a numerical estimate for EI, we assume the nanotube is an infinitely thin cylinder. This implies an aspect ratio of $\epsilon=\sqrt{2}L/R$

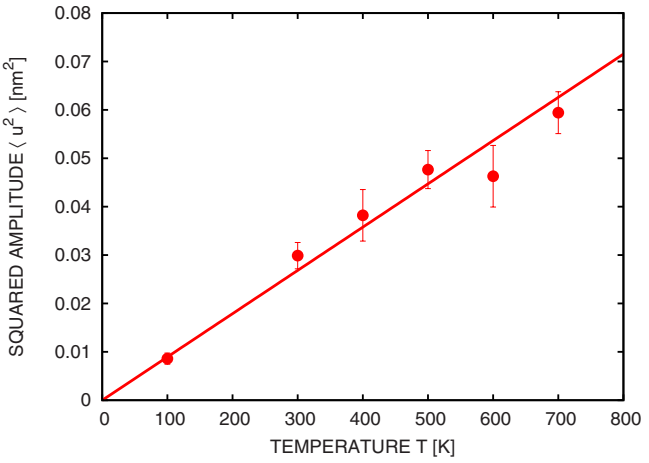

FIG. 2. (Color online) The thermal vibration width in nanometer squared versus temperature in Kelvin for a 20 nm tube. A best-fit line from a weighted least-squares analysis gives an intercept of 1.6608×10^{-4} nm^2 with an error of 1.4724×10^{-3} nm^2, confirming the linear hypothesis in Eq. (3). The best-fit line shown in the figure is constrained to have zero intercept.

≈ 40.4061. The theory of Cowper[15] gives $\kappa=4+3\nu$ for an infinitely thin cylinder; using a Poisson ratio $\nu=0.21$, a median representative value[25] taken from one of many existing theories, we obtain $\kappa=4.63$. These values give a flexural rigidity of $EI=4.0806\times10^{-25}$ N m^2. It is not possible to compare this result with previous estimates of the Young's modulus E since $I=0$ for an infinitely thin cylinder. However, if we analyze our data using the common assumption that the thickness of the tube is 0.34 nm, the interlayer spacing of graphene, we obtain an estimate of $E=1.070$ TPa. This value is in the range of values reported in previous experimental and computational work.[26]

In Fig. 1, the discrete impulses correspond to the modal frequencies of beam theory $\omega_n=\Omega_n L^{-3/2}\sqrt{EI/m}$ according to the Timoshenko theory while the green points are the EB theory. Since our classical approximation[16] for each mode is only valid for $\frac{\hbar\omega}{k_BT}\ll 1$, we show results for the Timoshenko and EB beam theories for $\frac{\hbar\omega}{k_BT}<0.05$. To within the error of our estimate of EI, given by the width of each impulse, the Timoshenko results accurately predict the location of the corresponding spectrum peak. The EB results are quantitatively similar to the Timoshenko results for the longer 50 nm CNT and at the fundamental mode of both CNTs due to the small $\Omega\epsilon^{-2}$ limit of Eq. (6). However, the EB theory shows significant discrepancies from the MD data at higher frequencies.

We also use Eq. (8) to predict the amplitude $\langle u_n^2\rangle$ of each mode. For the Timoshenko theory, this requires numerical quadrature to evaluate N_n in Eq. (7). In the limiting EB theory, $N_n=\frac{1}{4}$ so the amplitude scales as $\langle u^2\rangle\sim\omega^{-2}$. To make a comparison of an undamped beam theory with the MD results, we must account for the spreading of the peaks that results from the anharmonic interaction of phonon modes. In Fig. 1, we display a total intensity of each spectrum peak that corresponds to summing the spectrum between the midpoints to the two adjacent peaks, the discrete analog of integrating over the spectral intensity in Eq. (9). The Timoshenko results are remarkably accurate in predicting this total intensity of the MD results while the EB theory gives accurate results for the longer 50 nm CNT and at lower frequencies. Moreover, this analysis of the MD data shows that 97% of the total spectral intensity resides in the fundamental mode for the 20 and 50 nm CNTs. This result is confirmed by the Timoshenko theory in Eq. (8) for tubes of this length as well as by the limiting EB theory.[2]

V. DISCUSSION

To conclude, we return to the relationship between the tip vibrational spectrum and noise. For a cantilever, it is common assume the tip behaves as a harmonic oscillator corresponding to the cantilever's fundamental mode.[27] Within this model, the higher-order modes can be seen as a source of noise on the primary mode that arise from weak interactions between the modes. This noise causes the spreading and presumably shifting of the first peak in the spectrum that must be taken into account. Given the effects of these high-frequency features, it is important to make experimental measurements of the vibrational spectrum of the tip well above the first harmonic. This should be possible using the field emission properties of a CNT that have been employed in a radio[28] and a mass sensor.[7]

ACKNOWLEDGMENTS

We would like to acknowledge the support of the Laboratory Directed Research and Development program at Sandia National Laboratories. Sandia is a multiprogram laboratory operated by Sandia Corporation, a Lockheed Martin Co., for the United States Department of Energy under Contract No. DE-ACO4-94AL85000.

*ehfeng@sandia.gov

[1] M. M. J. Treacy, T. W. Ebbesen, and J. M. Gibson, Nature (London) **381**, 678 (1996).
[2] A. Krishnan, E. Dujardin, T. W. Ebbesen, P. N. Yianilos, and M. M. J. Treacy, Phys. Rev. B **58**, 14013 (1998).
[3] P. Poncharal, Z. Wang, D. Ugarte, and W. de Heer, Science **283**, 1513 (1999).
[4] R. Ciocan, J. Gaillard, M. Skove, and A. Rao, Nano Lett. **5**, 2389 (2005).
[5] D. Garcia-Sanchez, A. San Paulo, M. J. Esplandiu, F. Perez-Murano, L. Forro, A. Aguasca, and A. Bachtold, Phys. Rev. Lett. **99**, 085501 (2007).
[6] X.-L. Wei, Y. Liu, Q. Chen, M.-S. Wang, and L.-M. Peng, Adv. Funct. Mater. **18**, 1555 (2008).
[7] K. Jensen, K. Kim, and A. Zettl, Nat. Nanotechnol. **3**, 533 (2008).

[8] M. Viani, T. Schaffer, A. Chand, M. Rief, H. Gaub, and P. Hansma, J. Appl. Phys. **86**, 2258 (1999).
[9] D. A. Walters, J. P. Cleveland, N. H. Thomson, P. K. Hansma, M. A. Wendman, G. Gurley, and V. Elings, Rev. Sci. Instrum. **67**, 3583 (1996).
[10] B. I. Yakobson, C. J. Brabec, and J. Bernholc, Phys. Rev. Lett. **76**, 2511 (1996).
[11] H. Jiang, M. F. Yu, B. Liu, and Y. Huang, Phys. Rev. Lett. **93**, 185501 (2004).
[12] L. Wang and H. Hu, Phys. Rev. B **71**, 195412 (2005).
[13] J.-Y. Hsieh, J.-M. Lu, M.-Y. Huang, and C.-C. Hwang, Nanotechnology **17**, 3920 (2006).
[14] S. P. Timoshenko, Philos. Mag. **41**, 744 (1921).
[15] G. Cowper, J. Appl. Mech. **33**, 335 (1966).
[16] D. A. McQuarrie, *Statistical Mechanics* (Harper & Row, New York, 1976).
[17] T. Huang, J. Appl. Mech. **28**, 579 (1961).
[18] A. L. Fetter and J. D. Walecka, *Theoretical Mechanics of Particles and Continua* (McGraw-Hill, New York, 1980).
[19] J. Tersoff, Phys. Rev. B **37**, 6991 (1988).
[20] J. Tersoff, Phys. Rev. Lett. **61**, 2879 (1988).
[21] H. C. Andersen, J. Chem. Phys. **72**, 2384 (1980).
[22] C. Yu, L. Shi, Z. Yao, D. Li, and A. Majumdar, Nano Lett. **5**, 1842 (2005).
[23] D. Frenkel and B. Smit, *Understanding Molecular Simulation* (Academic, New York, 2001).
[24] M. P. Allen and D. J. Tildesley, *Computer Simulation of Liquids* (Clarendon, New York, NY, 1989).
[25] V. N. Popov, V. E. Van Doren, and M. Balkanski, Phys. Rev. B **61**, 3078 (2000).
[26] A. Sears and R. C. Batra, Phys. Rev. B **69**, 235406 (2004).
[27] D. Sarid, *Scanning Force Microscopy: With Applications to Electric, Magnetic, and Atomic Forces* (Oxford University Press, USA, 1994).
[28] K. Jensen, J. Weldon, H. Garcia, and A. Zettl, Nano Lett. **8**, 374 (2008).